Residual Stress Analysis of Self-lubricating Gradient Cemented Carbide Tool Material

Jingwei Xu[1], Siwen Tang[1*], Deshun Liu[2]

[1] Hunan Provincial Key Laboratory of Health Maintenance for Mechanical Equipment, Hunan University of Science and Technology, Xiangtan 411201, China

[2] Engineering Research Center of Advanced Mining Equipment, Ministry of Education, Hunan University of Science and Technology, Xiangtan 411201, China

Abstract：In this paper, the distribution of residual stress and the influence of the compositional distribution exponent, the number of gradient layers and thickness of gradient layer on the residual stress of Ni_3Al-TiC-WC-CaF_2 self-lubricating gradient cemented carbide tool material were analyzed by a finite element method. The results showed that the X-component stress in the gradient tool material was gradually changed from tensile stress to compressive stress, then transition to tensile stress, and finally the compressive stress was formed on the surface. Most of the area in the tool material was subjected to a small Y-component stress. The Z-component stress distribution was basically the same as that of the X-component stress. Under certain number of layers and gradient layer thickness conditions, the X-component stress of the gradient tool material changed with the increase of compositional distribution exponent n_1 and n_3, and that of the gradient tool material gradually changed from compressive stress to tensile stress with the increase of compositional distribution exponent n_2. The maximum Von Mises equivalent stress decreased first and then increased with the variation of the compositional distribution exponent. Under certain total thickness of gradient layer and compositional distribution exponent conditions, the X-component compressive stress of the surface of the gradient tool material increased with the increasing of the number of gradient layers, the maximum Von Mises equivalent stress value decreased with increasing of the number of gradient layers. The X-component compressive stress on the surface of the gradient tool material increased with

* Corresponding Author (siw_tang@hnust.edu.cn)

 ISSN 2572-4975 (Print), 2572-4991 (Online)

increasing of the thickness of the gradient layer under the condition that the compositional distribution exponent and the gradient number of layers were constant, and the maximum Von Mises equivalent stress decreased with increasing of the thickness of the gradient layer.

Key words：functionally graded material; cemented carbide; residual stress; finite element method

1 Introduction

With the rapid development of manufacturing industry, processing efficiency requirements of the industry continue to increase. The development of the tool has a direct impact on improving production efficiency and processing quality[1]. Cemented carbide tool has been widely used in high-speed machining, with outstanding performances: high strength, high toughness and high hardness, and good thermal stability and thermal stiffness[2]. TiC-WC was usually used as the basic material of cemented carbide tool, and it often uses Co as the bonding phase, but as a scarce resource, the use of Co is subjected to certain restrictions and it leads to higher raw material costs, and Co dust also has harmful effects on the environment and human health[3]. In comparison, Ni_3Al raw materials cost less and it is no pollution to the environment, and the Ni_3Al-based metal compound has good wettability with WC and TiC. The Ni_3Al/TiC and Ni_3Al/WC cemented carbides were prepared by vacuum sintering and hot pressing, and the TiC, WC particles were uniformly distributed in the semi-continuous Ni_3Al phase[4]. In addition, Ni_3Al has high hardness, high strength, high oxidation resistance and corrosion resistance and other excellent physical and mechanical properties as a bonded phase[5].

Although the traditional carbide cutting tools with high strength, high hardness, high wear resistance, its lubrication and anti-friction performance is poor, and it produce a lot of cutting heat easily, which influence the processing quality and the tool life in the high-speed dry cutting process seriously[6]. Xu et al[7] found that the addition of solid lubricants to the tool material can effectively reduce the friction coefficient and improve the friction and wear properties of the tool, thereby it can reducing the cutting heat caused by severe friction during high-speed dry cutting, and increasing tool life and processing surface quality. The results showed that CaF_2 is an

excellent high temperature solid lubricant, but the addition of solid lubricant will change the physical properties of the material, thus changing the distribution and size of residual stress. If the residual stresses are too large or unreasonable distribution will make the performance of the tool material to reduce or even failure. Functionally graded material (FGM) can continuously change the material composition, and it is a good way to alleviate the residual thermal stress[8], and can also make up for the above deficiencies. Therefore, this paper intends to use TiC-WC as the hard phase, and adding the solid lubricant CaF_2 through the component gradient to the tool material in order to enhance the lubricity of the tool material and improve the residual stress distribution of the tool material. The tool material is designed and the appropriate function gradient component distribution model is established in this paper firstly. Then the physical properties of the tool material are determined. The finite element simulation model is established to analyze the influence of the compositional distribution exponent, the gradient number of layers and thickness of gradient layer on the residual stress of the FGM. The results provide a theoretical basis for the preparation of high performance self-lubricating gradient cemented carbide tools.

2 Design of self-lubricating gradient cemented carbide tool material

2.1 Physical model

In order to facilitate the calculation, a diameter of 50mm, 19mm thick disc model is adopted, the model is symmetric about XOZ plane, with a 10mm thick matrix layer in the middle layer and the rest for the gradient layer, the model is shown in Fig. 1. Considering the symmetry of the model, take the X-Y rectangular section of the upper half of the center plane as the finite element model, and the coordinate origin is O. In order to accurately simulate the variation of the residual stress in the sample gradient layer region, the mesh density of the region is increased when the mesh is divided, as shown in Fig. 2. The calculated boundary conditions are: sintering temperature from 1700 ℃ to room temperature 20 ℃; the O point is pinned to limit any movement, the other edges are free.

 ISSN 2572-4975 (Print), 2572-4991 (Online)

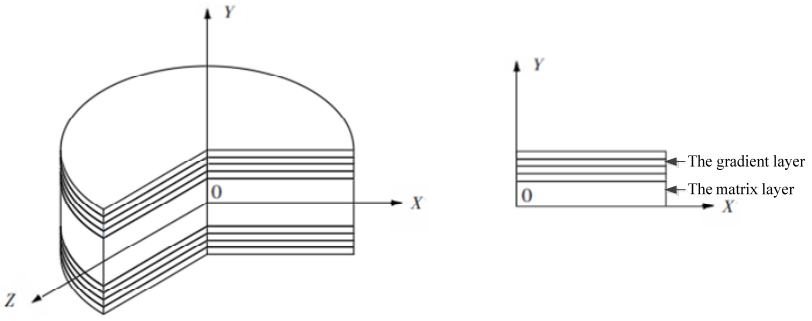

Fig.1. Physical model of self-lubricating gradient tool.

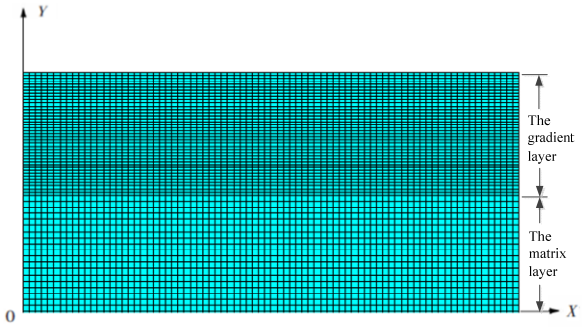

Fig.2. Finite element mesh model.

2.2 Material composition distribution model

Self-lubricating gradient materials are composed of solid lubricants and composite matrix materials. For Ni_3Al-TiC-WC-CaF_2 self-lubricating gradient cemented carbide tool material, it has three free phases. In order to make the tool material have the same mechanical properties on the top and bottom surfaces after sintering, symmetrical exponential distribution function was adapted in this paper[9]. The composition of the material changes symmetrically along the thickness direction, and it ignores the effects of stomata. First, the Ni_3Al-TiC-WC cemented carbide matrix is regarded as a component *m*, and the gradient distribution function of the volume fraction of CaF_2 along the thickness direction of the material is expressed by the following forms:

$$V_{CaF_2}(x)=\begin{cases}(V_1^{CaF_2}-V_0^{CaF_2})\left[\dfrac{0.5-x}{0.5}\right]^{n_1}+V_0^{CaF_2}\ 0\le x\le 0.5\\ (V_1^{CaF_2}-V_0^{CaF_2})\left[\dfrac{x-0.5}{0.5}\right]^{n_1}+V_0^{CaF_2}\ 0.5\le x\le 1\end{cases} \tag{1}$$

where, x is the ratio of the distance from the surface of the component to the gradient material to the total thickness of the tool material; $V_0^{CaF_2}$ and $V_1^{CaF_2}$ are the volume fraction of CaF_2 in the middle layer and surface layers respectively. n_1 is the functional gradient compositional distribution exponent of CaF_2 in the tool material.

The volume fraction distribution function of the matrix element m is

$$V_m=1-V_{CaF_2} \tag{2}$$

In the matrix material m, TiC-WC as a component p, the volume fraction of Ni_3Al obeys the function gradient compositional distribution exponent n_2, the expression is:

$$V_{Ni_3Al}(x)=\begin{cases}\left(V_1^{Ni_3Al}-V_0^{Ni_3Al}\right)\left[\dfrac{0.5-x}{0.5}\right]^{n_2}+V_0^{Ni_3Al}\ 0\le x\le 0.5\\ \left(V_1^{Ni_3Al}-V_0^{Ni_3Al}\right)\left[\dfrac{x-0.5}{0.5}\right]^{n_2}+V_0^{Ni_3Al}\ 0.5\le x\le 1\end{cases} \tag{3}$$

where, $V_0^{Ni_3Al}$ and $V_1^{Ni_3Al}$ are the volume fraction of Ni_3Al in the middle layer and surface layers respectively. n_2 is the functional gradient compositional distribution exponent of Ni_3Al in the tool material.

Therefore, the volume fraction of TiC-WC composite phase components is:

$$V_n=1-V_{CaF_2}-V_{Ni_3Al} \tag{4}$$

In p, the WC as a free phase, then the volume fraction of WC obeys the function gradient compositional distribution exponent n_3, the expression is:

$$V_{WC}(x)=\begin{cases}\left(V_1^{WC}-V_0^{WC}\right)\left[\dfrac{0.5-x}{0.5}\right]^{n_3}+V_0^{WC}\ 0\le x\le 0.5\\ \left(V_1^{WC}-V_0^{WC}\right)\left[\dfrac{x-0.5}{0.5}\right]^{n_3}+V_0^{WC}\ 0.5\le x\le 1\end{cases} \tag{5}$$

Where V_0^{WC} and V_1^{WC} are the volume fraction of WC in the middle layer and surface layers respectively, n_3 is the functional gradient compositional distribution

 ISSN 2572-4975 (Print), 2572-4991 (Online)

exponent of WC in the tool material.

In the multicomponent self-lubricating functionally graded cemented carbide material, the volume fraction distribution function of TiC is expressed by the following forms:

$$V_{TiC}(x)=1-V_{CaF_2}(x)-V_{Ni_3Al}(x)-V_{WC}(x) \tag{6}$$

In order to ensure the overall strength and hardness of the tool material, the intermediate matrix layer does not contain the solid lubricant CaF_2[10], the surface volume of CaF_2 does not exceed 15%. For the Ni_3Al-TiC-WC-CaF_2 self-lubricating gradient cemented carbide tool material, the thermal expansion coefficient of TiC/WC is smaller than that of Ni_3Al. In order to gradually reduce the thermal expansion coefficient of the functionally graded tool material from the matrix to the surface layer, the content of TiC/WC in the matrix material Ni_3Al/TiC/WC should be increased from the middle layer to the two surface layers. Therefore, Ni_3Al and WC in the middle layer and surface content were taken as 10%, 40% and 45%, 25% respectively. So this article take $V_0^{CaF_2}=0$, $V_1^{CaF_2}=15\%$, $V_0^{Ni_3Al}=40\%$, $V_1^{Ni_3Al}=10\%$, $V_0^{WC}=45\%$, $V_1^{WC}=25\%$.

2.3 Material properties model

When calculating the thermal stress of the FGM, it is necessary to determine the physical properties of each gradient layer material, including elastic modulus, thermal expansion coefficient, Poisson's ratio and thermal conductivity. At present, these parameters are mainly approximated by the mixed law of the material[11]. However, this general hybrid rule does not take into account the real microstructure and porosity of the material, there is a certain error. Therefore, the material properties (E, α, μ) in this paper are given by Mori-Tanka's theory[12] and Kerner's equation[13], and the thermal conductivity k is given by Kingery's equation[14]:

$$K_x=K_A\left[1+\frac{V_B(x)(K_B-K_A)}{K_A+a(1-V_B(x))(K_B-K_A)}\right] \tag{7}$$

$$G_x=G_A\left[1+\frac{V_B(x)(G_B-G_A)}{G_A+b(1-V_B(x))(G_B-G_A)}\right] \tag{8}$$

Where K_x is the equivalent volume modulus at x in the gradient layer; Where G_x is the

equivalent shear modulus at x in the gradient layer; $V_A(x)$, $V_B(x)$ is the volume fraction of A and B component at x, where $V_A(x)+V_B(x)=1$; K_A, K_B is the basic bulk modulus of the A and B components: $K_A=\frac{E_A}{3(1-2\mu_A)}$, $K_B=\frac{E_B}{3(1-2\mu_B)}$; G_A, G_B is the basic shear modulus of the A and B components: $G_A=\frac{E_A}{2(1+\mu_A)}$, $G_B=\frac{E_B}{2(1+\mu_B)}$, $a=\frac{1+\mu_A}{3(1-\mu_A)}$, $b=\frac{2(4-5\mu_A)}{15(1-\mu_A)}$.

The elastic modulus at x in the gradient layer

$$E_x=\frac{9K_xG_x}{3K_x+G_x} \tag{9}$$

The Poisson's ratio at x in the gradient layer

$$\mu_x=\frac{3K_x-2G_x}{2(3K_x+G_x)} \tag{10}$$

The thermal expansion coefficient at x in the gradient layer

$$\alpha_x=\alpha_A+\frac{V_B(x)(\alpha_B-\alpha_A)}{\frac{12K_AG_A}{3K_A+4G_A}\left[\frac{V_B(x)}{3K_A}+\frac{1}{4G_A}+\frac{1-V_B(x)}{3K_B}\right]} \tag{11}$$

Where α_A, α_B is the basic coefficient of thermal expansion of the A and B components.

The thermal conductivity at x in the gradient layer

$$k_x=k_A\frac{1+2V_B(x)\left(1-\frac{k_A}{k_B}\right)\Big/\left(\frac{2k_A}{k_B}+1\right)}{1-V_B(x)\left(1-\frac{k_A}{k_B}\right)\Big/\left(\frac{k_A}{k_B}+1\right)} \tag{12}$$

Where k_A, k_B are the basic thermal conductivity of the A and B components.

The volume fraction distribution functions $V_{Ni_3Al}(x)$, $V_{TiC}(x)$, $V_{WC}(x)$ and $V_{CaF_2}(x)$ of the matrix components Ni_3Al, TiC, WC and the solid lubricant CaF_2 are substituted into the Eq. (9), (10), (11) and (12) respectively, the distribution functions $E(x)$,

 ISSN 2572-4975 (Print), 2572-4991 (Online)

$\mu(x)$, $\alpha(x)$ and $k(x)$ of the elastic modulus, Poisson's ratio, thermal expansion coefficient and thermal conductivity along the gradient direction are obtained. The physical properties of raw materials are shown in Table 1.

Tab. 1. The physical properties of raw materials[15].

Raw materials	Elastic modulus	Thermal expansion coefficient	Poisson's ratio	Thermal conductivity
	E/GPa	$\alpha/\times10^{-6}K^{-1}$	μ	$\kappa/\mathrm{w}\times(\mathrm{mk})^{-1}$
Ni_3Al	179	12.5	0.295	28.85
TiC	450	7.6	0.19	24.28
WC	719	6.9	0.23	15.55
CaF_2	75.8	18.85	0.26	9.71

In the calculation of residual stress, it is assumed that the interface of each gradient layer is well bonded and its physical properties are isotropic and do not change with the temperature[16]. The model is adiabatically, and there is no heat source inside the material.

3 Results and discussion

3.1 Distribution of residual stress

Fig. 3 shows the X-component stress distribution with the compositional distribution exponent taken n_1=4; n_2=n_3=1. It can be seen from fig. 3a that the X-component stress gradually became compressive stress from the tensile stress, and then switched to the tensile stress, finally compressive stress was formed on the surface. The maximum compressive stress appeared in the matrix next to the gradient layer, and the maximum tensile stress appeared in the middle of the gradient layer. The stress on the side of the material was small. The X-component stress on the surface of the self-lubricating gradient cemented carbide tool material was shown in fig. 3b. It can be seen from fig. 3b that there was a uniform distribution of compressive stress in the area of x<17.5mm; when x≥17.5mm, the compressive stress increased first and reached the maximum value(-154Mpa) at x=19.5mm, then it

sharply reduced and tended to zero, which was consistent with the trend of residual stress in[7]. Fig.4 shows the Z-component stress distribution with the compositional distribution exponent taken n_1=4; n_2=n_3=1. It can be seen from fig. 4a that the Z-component stress distribution of the tool material was basically the same as that of the X-component stress. However, the stress on the side of the material was reduced. The Z-component stress on the surface of the tool material was shown in fig. 4b. It can be seen from fig. 4b that the compressive stress was uniformly distributed in the area of x<16mm; when x≥16mm, the compressive stress increased first, and reached the maximum value (-149Mpa) at x=19.5mm, then it decreased gradually, At the edge there was still compressive stress(-104MPa).

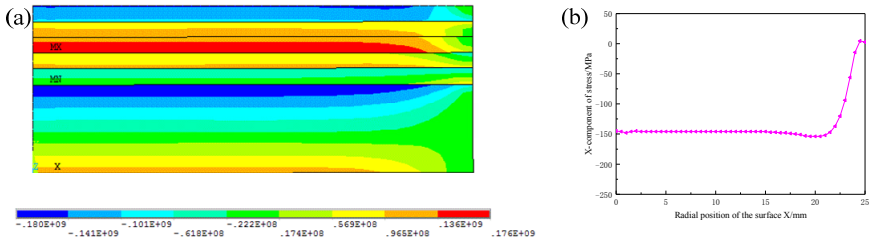

(a) The contour maps of X-component stress; (b) X-component stress distribution on the surface of the material.

Fig. 3. X-component stress distribution.

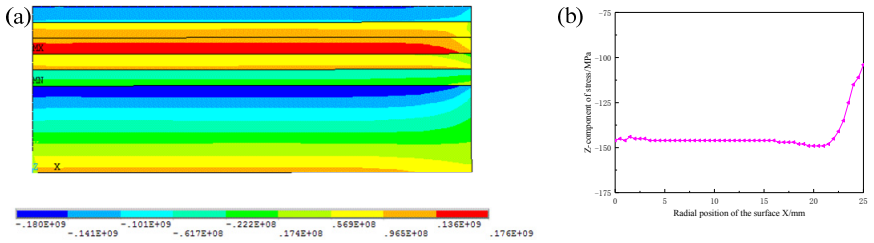

(a) The contour maps of Z-component stress; (b) Z-component stress distribution on the surface of the material.

Fig. 4. Z-component stress distribution

Fig. 5 shows the Y-component stress distribution with the compositional distribution exponent taken n_1=4; n_2=n_3=1. It can be seen from fig. 5a that in the self-lubricating gradient cemented carbide tool material, most of the area withstood

 ISSN 2572-4975 (Print), 2572-4991 (Online)

the smaller Y-component stress, at the side of the tool which was subjected to a greater tensile and compressive stresses. The maximum compressive stress appeared on the side of the gradient layer, and the maximum tensile stress appeared on the side of the matrix next to the gradient layer. The Y-component stress on the side of the tool material was shown in fig. 5b. It can be seen from fig. 5b that the Y-component stress was very small at the bottom of the matrix (close to 0), with the increase of the axial position, Y-component tensile stress gradually increased, and it reached the maximum value(139MPa) at y=4.5mm, then it gradually reduced to the increased compressive stress which reached the maximum value(-149MPa) at the position of y=7.25mm, and then gradually reduced to almost zero.

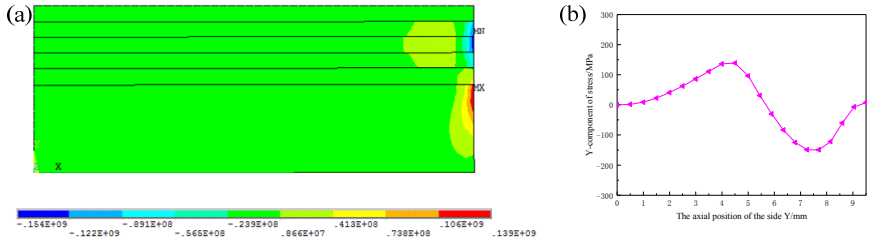

(a) The contour maps of Y-component stress; (b) Y-component stress distribution on the side of the material.

Fig. 5. Y-component stress distribution.

3.2 The influence of compositional distribution exponent on residual stress

3.2.1 The influence of compositional distribution exponent on X-component stress

With different compositional distribution exponent *n*, the ways of transition for physical properties of the gradient layer are different, which causes different residual stress distributions. The residual stress was calculated by the gradient tool material with *d*=0.9mm and *N*=5, and the effect of n on the residual stress was discussed.

The residual compressive stress on the tool surface can counteract the mechanical stress generated during the cutting process and improve the cutting performance of the tool[13]. Fig. 6 shows the curves of the X-component stress mean value under uniform distribution on the surface of gradient tool material with different

compositional distribution exponent.

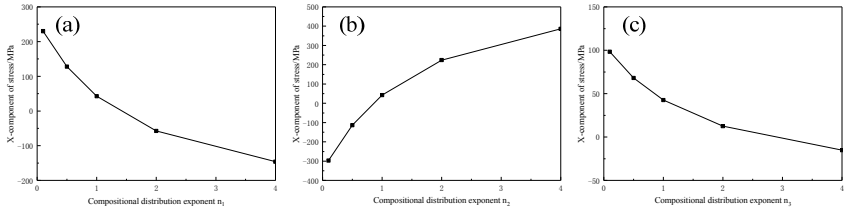

(a) the effect of n_1 on the X-component stress (n_2=n_3=1); (b) the effect of n_2 on the X-component stress (n_2=n_3=1); (c) the effect of n_3 on the X-component stress (n_2=n_3=1).

Fig. 6. Relationship between the X-component stress and the compositional distribution exponent.

It can be seen from fig. 6a that with the increase of n_1, the X-component stress changed from tensile stress to compressive stress. When $n_1 \leq 1$, there was tensile stress on the surface of the gradient tool material, and with the increase of n_1, the X-component tensile stress of this region decreased gradually. When $n_1 > 1$, it changed into compressive stress, and as n_1 continues to increase, the X-component compressive stress increased further. It can be seen from fig. 6b that, as n_2 increases, the X-component stress changed from compressive stress to tensile stress. When $n_2 < 1$, there was compressive stress on the surface of the gradient tool material. When n_2=0.1, the maximum compressive stress was 297MPa, and with the increase of n_2, the X-component compressive stress of this region decreased gradually; when $n_2 \geq 1$, it became the tensile stress, and with the increase of n_2, the X-component tensile stress was also increased. From fig. 6c, it can be seen that with the increase of n_3, the X-component stress was changed from tensile stress to compressive stress. When $n_3 \leq 2$, there was tensile stress on the surface of the gradient tool material, and with the increase of n_3, the X-component tensile stress was gradually reduced. When $n_3 > 2$, there was compressive stress.

3.2.2 The influence of compositional distribution exponent on maximum Von Mises equivalent stress

The maximum Von Mises equivalent stress of the gradient tool material under different compositional distribution exponent was shown in fig. 7. It can be seen from

 ISSN 2572-4975 (Print), 2572-4991 (Online)

the figure that the variation trend of the maximum Von Mises equivalent stress affected by n_1, n_2, n_3 were basically the same, which all decreased first and then increased. When n_1, n_2 and n_3 were 1, the minimum value was 130MPa. The maximum Von Mises equivalent stress was most affected by n_2, followed by n_1, and the least affected was n_3. As n_2, n_1, n_3 were less than 1 respectively, the rate of reduction for the maximum Von Mises equivalent stress became less orderly with the growth of its compositional distribution exponent. As n_3, n_1, n_2 were greater than or equal to 1 respectively, the rate of increase for the maximum Von Mises equivalent stress became greater with the growth of its compositional distribution exponent.

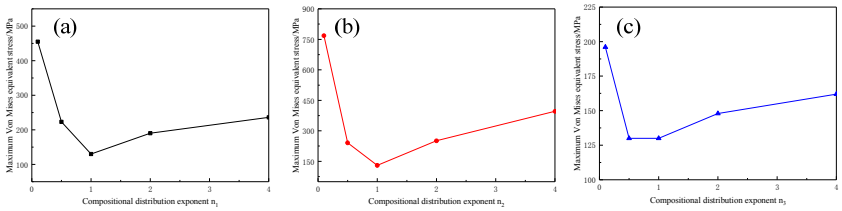

((a) the effect of n_1 on the maximum Von Mises equivalent stress; (b) the effect of n_2 on the maximum Von Mises equivalent stress; (c) the effect of n_3 on the maximum Von Mises equivalent stress.)

Fig. 7. Relationship between the maximum Von Mises equivalent stress and the compositional distribution exponent.

3.3 The influence of gradient layers on residual stress

3.3.1 The influence of gradient layers on X-component stress

Fig. 8 shows the curves of the X-component stress mean value under uniform distribution on the surface of the gradient tool material under different gradient layers (the total thickness of the gradient layer is 4.5mm and the compositional distribution exponent is n_1=4; n_2=n_3=1). It can be seen from the figure that the X-component compressive stress of the surface of the gradient tool material increased with the increasing N; When N≥5, the X-component of compressive stress changed a little with the increasing of N. When the N increased to 9 layers, the surface compressive stress reached the maximum value(-148MPa), and when N continues to increase, the compressive stress began to decrease.

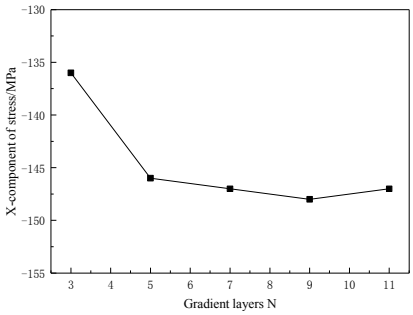

Fig. 8. Relationship between the X-component stress and gradient layers.

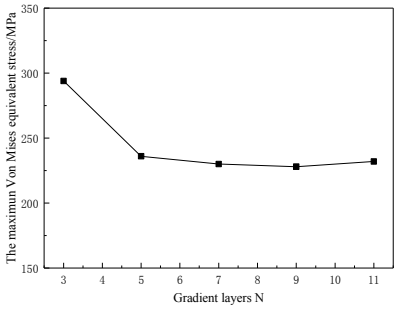

Fig. 9. Relationship between the maximum Von Mises equivalent stress and gradient layers.

3.3.2 The influence of gradient layers on maximum Von Mises equivalent stress

The maximum Von Mises equivalent stress variation curve of the gradient tool material under different number of gradient layers was shown in fig. 9. With the increase of *N*, the maximum Von Mises equivalent stress tended to decrease. When *N* was increased from 3 to 5, the maximum Von Mises equivalent stress was dropped from 294 MPa to 236 MPa, and decreased by 19.7%, and it had little change when after 5 layers. When the number of gradient layer was 9, the minimum value was 228Mpa, the maximum Von Mises equivalent stress was slightly increased to 232 MPa when the gradient layer was increased to 11 layers.

From the above analysis, it can be seen that with the increase of the number of layers, the residual stress of the gradient tool material tended to be smooth, and the compressive stress on the surface of the gradient layer was increased, which was beneficial to improve the overall performance of the material. However, the more

gradient layers, the more difficult it is to prepare. It can be seen from fig. 9 that when the gradient layer was larger than 5 layers, a better residual stress relaxation effect can be obtained.

3.4 The influence of gradient layer thickness on residual stress

3.4.1 The influence of gradient layer thickness on residual stress

Fig.10 shows the curves of the X-component stress mean value under uniform distribution on the surface of the gradient tool material under different gradient layer thickness (the number of gradient layers is 5 and the compositional distribution exponent is n_1=4; n_2=n_3=1). It can be seen from the figure that the surface of the tool material was tensile stress only when d=0.3mm. When d≥0.5mm, the X-component compressive stress of the surface of the tool material increased with the increasing of d. When d increased from 0.5mm to 1.1mm, the compressive stress increased from -62.3MPa to -167MPa, increased by 168.1%.

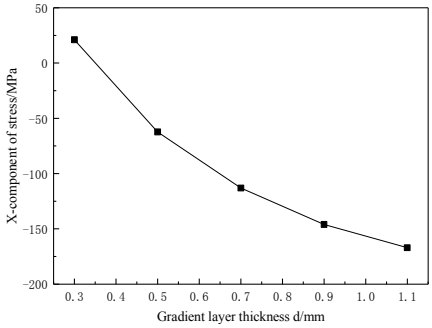

Fig. 10. Relationship between the X-component stress and gradient layer thickness.

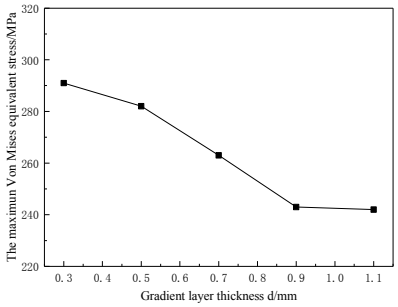

Fig. 11. Relationship between the maximum Von Mises equivalent stress and gradient layer thickness.

3.4.2 The influence of gradient layer thickness on maximum Von Mises equivalent stress

The maximum Von Mises equivalent stress variation curve of the gradient tool material at different gradient layer thickness is shown in fig. 11. It is shown that with the increasing of *d*, the maximum Von Mises equivalent stress was gradually decreased, when the *d* reached to 0.9mm, the maximum Von Mises equivalent stress decreased from 291MPa to 243MPa, downed by 16.5%, the gradient layer thickness continues to increase and the stress relaxation effect was no longer obvious. In summary, the increase in the thickness of the gradient layer can refine the distribution of the composition of the material, so that the transition of physical properties of the gradient material became smoother, and the trend of stress change became moderate, thus it can avoid stress concentration caused by excessive mismatch of material properties.

4 Conclusion

In this paper, the distribution law of residual stress and the influence of compositional distribution exponent *n*, the number of gradient layers *N* and thickness of gradient layer *d* on residual stress were analyzed by finite element method in Ni_3Al-TiC-WC-CaF_2 self-lubricating gradient cemented carbide tool material. The results were as follows:

(1) The X-component stress in the gradient tool material was gradually changed from tensile stress to compressive stress, and then turned to tensile stress, from the bottom surface of the matrix to the surface of the gradient layer, and finally the compressive stress was formed on the surface. The Z-component stress distribution was basically the same as that of the X-component stress. Most of the area in the gradient tool material underwent a small Y-component stress.

(2) Under certain number of layers and gradient layer thickness conditions, the X-component stress of the gradient tool material gradually changed from tensile stress to compressive stress with the increase of compositional distribution exponent n_1 and n_3, and that of the gradient tool material gradually changed from compressive stress to tensile stress with the increase of compositional distribution exponent n_2. The variation trend of the maximum Von Mises equivalent stress affected by n_1, n_2, n_3 are decreased at first and then increased. The maximum Von Mises equivalent stress was

 ISSN 2572-4975 (Print), 2572-4991 (Online)

most affected by n_2, followed by n_1, and the least affected was n_3.

(3) The X-component compressive stress of the surface of the gradient tool material increased with the increasing of N under certain gradient layer of the total thickness and the compositional distribution exponent condition. When N>5, the compressive stress was no longer changes. The maximum Von Mises equivalent stress value of the gradient tool material decreases as N increases. When N was increased from 3 to 5, the maximum Von Mises equivalent stress was reduced by 19.7%, and when N>5, it had little change.

(4) Under the condition that the compositional distribution exponent and the gradient number of layers were certain, the X-component compressive stress in the surface of the gradient tool material increased with the increasing of d. When d increased from 0.5mm to 1.1mm, the compressive stress increased by 168.1%. The maximum Von Mises equivalent stress decreased with the increasing of d. When d reached to 0.9mm, the maximum Von Mises equivalent stress dropped by 16.5%, and when d>0.9, with the increase of the thickness of the gradient layer, the increase of the stress is no longer obvious.

Acknowledgement

This work was financially supported by the National Natural Science Foundation of China (Grant Nos. 51305134 and 51605161), and a Foundation of Hunan University of Science and Technology (grant no.E56128).

References

1 Kristen B. High-performance coatings for cutting tools, ***CIRP Journal of Manufacturing Science and Technology*** 18(2017)1-9.

2 Tang S, Liu D, Li P, et al. Microstructure and Mechanical Properties of Ti (C, N)-based Functional Gradient Cermets Nitriding by Microwave Heating, ***High Temperature Materials and Processes*** 34(2015) 457-460.

3 Norgren S, Garcia J, et al. Trends in the P/M hard metal industry, ***International Journal of Refractory Metals and Hard Materials*** 48(2015) 31-45.

4 Tiegs T. N, Alexander K. B, Plucknett K. P, et al. Ceramic composites with a ductile Ni_3A1 binder phase, ***Mater. Sci. Eng*** A209 (1996) 243-247.

5 Ahmadian M, Wexlar D. Liquid phase sintering of WC-Al and WC-Al composites with

and without boron, ***Materials Soienc; e Forum*** 32 (2003) 1951-1956.

6 Tang S, Liu D, Li P, et al. Formation of wear-resistant graded surfaces on titanium carbonitride-based cermets by microwave assisted nitriding sintering, ***International Journal of Refractory Metals & Hard Materials*** 48(2015) 217-221.

7 Xu C, Xiao G, et al. Finite element design and fabrication of Al_2O_3/TiC/CaF_2 gradient self-lubricating ceramic tool material, ***Ceramics International*** 40(2014) 10971-10983.

8 Tang S, Liu D, Li P, et al. Microstructure and mechanical properties of functionally gradient cemented carbides fabricated by microwave heating nitriding sintering, ***International Journal of Refractory Metals & Hard Materials*** 58(2016) 137-142.

9 Ai X, Zhao J, Huang C Z. et al. Development of an advanced ceramic tool material-functionally gradient cutting ceramics, ***Materials Science and Engineering A***, 248(1998) 125-131.

10 Deng J, Cao T, et al. Self-lubrication of sintered ceramic tools with CaF_2 additions in dry cutting, ***Int. J. Mach. Tool Manuf*** 46(2006) 957-963.

11 Wakashima K, Hirano T, Niino M. Space application of advance structure materials, ***Proc Int Symp Space Technol Sci*** (1990) 501-504.

12 Mori T, Tanaka K. Average stress in matrix and average elastic energy of materials with misfitting inclusions, ***Acta Metalh*** 21(1973) 571.

13 Kerner E H. The Elastic and Thermo-Elastic Properties of Composite Media, ***Proclamation of Physics Society*** 69B(1956) 808-813.

14 Kingery W D. The thermal conductivity of ceramic dielectrics, ***Progress in Ceramic Science*** 2(1962) 181-235.

15 Zhang L M. Properties of TiC-Ni_3Al composites and structural optimization of TiC-Ni_3Al functionally gradient materials, ***Materials Science and Engineering A*** 203(1995) 272-277.

16 Deng J, Duan Z, et al. Fabrication and Performance of Al_2O_3 /(W, Ti) C + Al_2O_3 /TiC Multilayered Ceramic Cutting Tools, ***Mat Sci Eng A*** 527(2010) 1039-1047.

 ISSN 2572-4975 (Print), 2572-4991 (Online)